Tectonophysics xxx (2009) xxx–xxx

Contents lists available at ScienceDirect

Tectonophysics

journal homepage: www.elsevier.com/locate/tecto

The nature and timing of crustal thickening in Southern Tibet: Geochemical and zircon Hf isotopic constraints from postcollisional adakites

Sun-Lin Chung [a,*], Mei-Fei Chu [a,b], Jianqing Ji [c], Suzanne Y. O'Reilly [b], N.J. Pearson [b], Dunyi Liu [d], Tung-Yi Lee [e], Ching-Hua Lo [a]

[a] Department of Geosciences, National Taiwan University, Taipei 106, Taiwan
[b] ARC National Key Centre GEMOC, Department of Earth and Planetary Sciences, Macquarie University, Sydney, NSW 2109, Australia
[c] School of Earth and Space Sciences, Peking University, Beijing 100871, China
[d] Institute of Geology, Chinese Academy of Geological Sciences, Beijing 100037, China
[e] Department of Earth Sciences, National Taiwan Normal University, Taipei 116, Taiwan

ARTICLE INFO

Article history:
Received 1 May 2008
Received in revised form 27 July 2009
Accepted 5 August 2009
Available online xxxx

Keywords:
Tibet
India–Asia collision
Postcollisional adakite
Basaltic underplating
Crustal thickening
Neotethyan subduction

ABSTRACT

Rising as "the roof of the world" the Tibetan plateau is now underlain with the thickest continental crust on Earth. How and when was this crust formed, which would have exerted pivotal controls to the formation of the plateau, has long been an issue of hot debates. This paper reports zircon U–Pb ages and Hf isotope data for postcollisional (~30–9 Ma) adakites in the southern Lhasa terrane, southern Tibet. A comparative analysis of whole-rock rare earth element geochemistry and zircon Hf isotopes between the adakites and associated Gangdese igneous rocks suggests that the Tibetan crust underwent a major phase of tectonic thickening between ca. 45 and 30 Ma in the region. The lower part of the thickened crust consisted prevailingly of mafic lithologies, which we argue to have resulted from intense basaltic underplating and subsequent remelting that took place during the Late Cretaceous and Eocene time related to the Neotethyan subduction processes including breakoff of the subducted slab at ca. 50 Ma in the early stage of the India–Asia collision. These processes were responsible for not only the juvenile crust formation but also for the creation of a thermally softened lithosphere in the southern Lhasa terrane. The indentation of India, consequently, caused distributed lithospheric thickening with formation of an orogenic root beneath southern Tibet. Root foundering during the Oligocene gave rise to the adakitic magmatism, regional topographic uplift, and onset of northward underthrusting of the Indian plate that has since played a key role in forming the entire Tibetan plateau.

1. Introduction

The Himalayan–Tibetan orogen produced by the continental collision between India and Asia is the most outstanding natural laboratory for studying the complex geologic processes through which collisional orogeny evolves. Many fundamental questions, nevertheless, still persist in our understanding of the formation of this most spectacular topographic feature on modern Earth. For example, although the presence of anomalously thick continental crust under the Tibetan plateau has been known for years (e.g., Allegrè et al., 1984), how and when such a thick crust was generated remains highly controversial. Prominent hypotheses that have been proposed for producing the thick crust, and the immense plateau, include (1) homogeneous pure-shear thickening of the entire Asian lithosphere because of the Indian indentation (e.g., England and Houseman, 1985; Houseman and Molnar, 1997), (2) injection of part or even all of the Indian continental crust into the Asian lower crust (Zhao and Morgan, 1987; Chemenda et al., 2000), and (3) underthrusting of the Indian lithospheric mantle and its lower crust beneath the Tibetan plateau (Owens and Zandt, 1997; Chemenda et al., 2000; DeCelles et al., 2002; Haines et al., 2003). Structural geologic data (Murphy et al., 1997; Kapp et al., 2005) suggest that substantial crustal shortening and thickening may have already taken place in southern Tibet before the India–Asia collision.

In this article, we present zircon U–Pb ages and in-situ Hf isotopes for postcollisional adakites in southern Tibet in the hope to better understand when and how the thick Tibetan crust was formed. These new results, together with our published and unpublished data from the region, lead us to concur with the suggestion: (1) there was a significant in-situ phase of crustal thickening from ca. 45 to 30 Ma, and (2) Cretaceous–Paleogene basaltic underplating and remelting related to the Neotethyan subduction played a controlling role in the Tibetan crustal thickening. These furthermore allow us to argue that in southern Tibet the lithosphere was relatively hot and soft prior to the India's hard indentation so that it underwent distributed pure-shear thickening at the early stage of the India–Asia collision.

* Corresponding author. Department of Geosciences, National Taiwan University, Taipei P. O. Box 13-318, Taipei 10617, Taiwan. Fax: +886 2 2363 6095.
E-mail address: sunlin@ntu.edu.tw (S.-L. Chung).

0040-1951/$ – see front matter © 2009 Elsevier B.V. All rights reserved.
doi:10.1016/j.tecto.2009.08.008

2. Postcollisional adakites in Southern Tibet

The term "adakite" was first proposed by Defant and Drummond (1990) to describe subduction-related volcanic and plutonic rocks of andesite to sodic rhyolite compositions that exhibit geochemical characteristics suggesting an origin by partial melting of hydrated mafic source rocks in the form of eclogite or garnet amphibolite (e.g., Kay, 1978; Rapp et al., 1991; Martin, 1999). Adopting the geochemical criteria by Defant and Drummond (1990), Chung et al. (2003) reported the first example of "collision-type" adakites from southern Tibet, which has been followed by a number of more recent studies (e.g., Hou et al., 2004; King et al., 2007; Guo et al., 2007; Gao et al., 2007; Aitchison et al., 2009) and provided important new clues that help improve our understanding of the Himalayan–Tibetan orogenesis. Nonetheless, there were different mechanisms proposed for the adakite generation in southern Tibet, which are summarized by the end of this section.

In southern Tibet (Fig. 1), the collision-type adakites occurred as small-volume plugs or dikes/sills, which intrude or crosscut the Gangdese batholith, Linzizong volcanic successions and associated sedimentary formations, with occurrence extending ~1300 km across nearly the entire Lhasa terrane. Radiometric age results, obtained mainly by Ar–Ar and zircon U–Pb dating methods (Coulon et al., 1986; Turner et al., 1996; Miller et al., 1999; Yin and Harrison, 2000; Williams et al., 2001; Chung et al., 2003; Spicer et al., 2003; Nomade et al., 2004; Hou et al., 2004; Williams et al., 2004; King et al., 2007; Aitchison et al., 2009), indicate that these adakites were emplaced between ca. 26 and 9 Ma. The magmatism actually started in the Zedong area (Fig. 1), where a slightly deformed intrusion called the Yaja granodiorite displaying adakitic geochemical features (Chung et al., 2005) was emplaced as early as ca. 30 Ma (Harrison et al., 2000; this study). The Tibetan adakites have intermediate to silicic composition ($SiO_2 \approx 56$–72 wt.%) and are mostly Na-rich, although K-rich varieties exist in several localities (Chung et al., 2003; Hou et al., 2004; Gao et al., 2007; Guo et al., 2007). Their overall geochemical features, marked by high Sr (to ~1100 ppm), low Y (<10 ppm) and heavy rare earth elements (REE), and thus strongly fractionated REE patterns (Fig. 2), coupled with depletions in the high field strength elements (e.g., Nb, Ta and Ti) and absence of negative Eu anomalies, are comparable to those of "type-locality" adakites from the circum-Pacific subduction zones (Defant and Drummond, 1990). These geochemical features are consistent with a magma origin from partial melting of garnet-containing mafic source rocks, e.g., eclogite or garnet amphibolite, that existed in the lower part of collision-thickened Tibetan crust (Chung et al., 2003; Hou et al., 2004; Guo et al., 2007). The widespread adakite magmatism postdating the onset of the India–Asia collision requires specific heat source, which has been widely ascribed to convective removal, or "delamination", of the lower part of the lithosphere under southern Tibet and its replacement by the hotter asthenosphere causing elevation of the geotherm (e.g., England and Houseman, 1989; Turner et al., 1996; Williams et al., 2001; Chung et al., 2003; Hou et al., 2004; Chung et al., 2005; Guo et al., 2007).

Instead of the general consensus on a mafic lower crust source region, Gao et al. (2007) argued that the adakitic magmas in southern Tibet were derived from an upper mantle source metasomatized by slab-released melts in the Neotethyan subduction. These authors, however, did not explain why there are no mafic rocks in association with the Tibetan adakitic suite if the mantle source indeed played a direct role in the magma genesis. King et al. (2007), based on their finding of mid-Miocene dacitic/adakitic dikes a few kilometers south of the Indus-Tsangpo suture, postulated a petrogenetic link with the mid-crustal ductile channel structure beneath southern Tibet (Beaumont et al., 2001; Jamieson et al., 2004). Thus, they argued the adakites to be crustal melts derived largely from the mid-lower crust (~30–40 km) of the Asian plate, exposed today as the Nyainqentanglha gneisses that underlie the Gangdese batholiths. This argument of a principal source from the mid-crustal gneisses, without garnet as the residual phase in partial melting, however, can hardly account for the HREE depletion and highly fractionated REE pattern of the adakites. Aitchison et al. (2009), with the conjecture of a late (ca. 35 Ma) rather than early (≥55 Ma) collision between India and

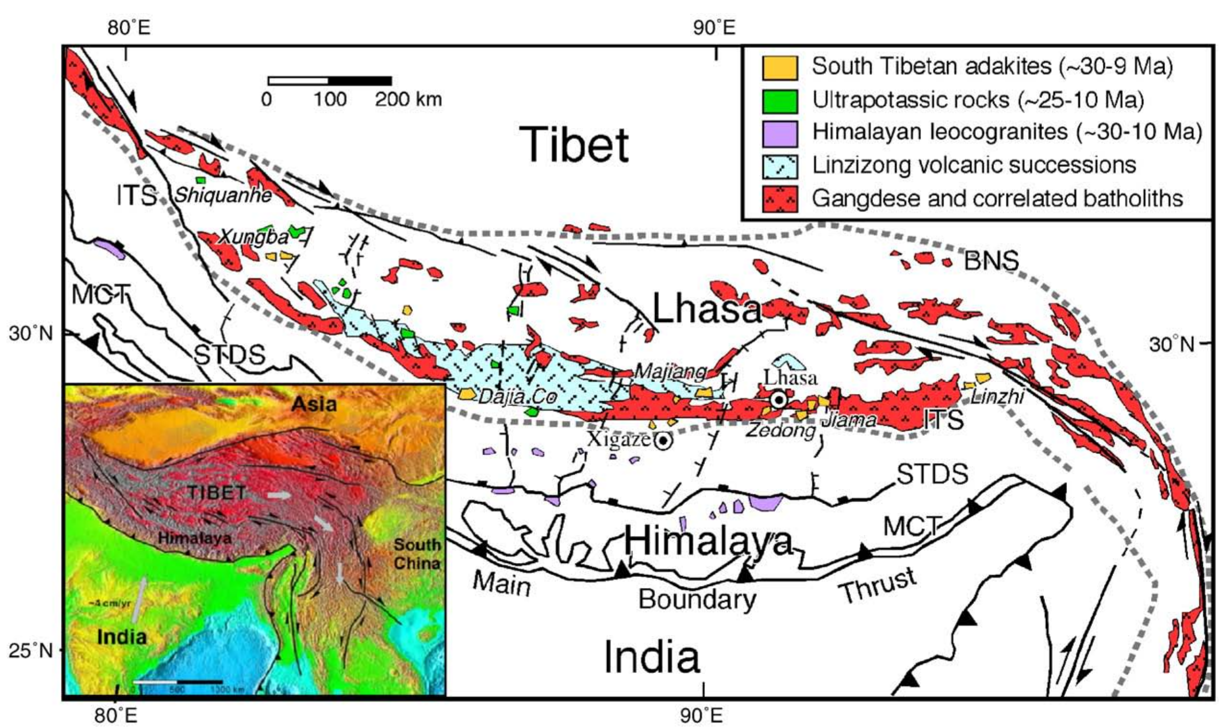

Fig. 1. Simplified geologic map showing outcrops of magmatic rocks in southern Tibet made essentially of the Lhasa terrane (modified from Chung et al., 2003; Lee et al., this volume). Sampling localities of the five adakites of this study, from west to east, are Majiang (T060B), Zedong (ST107A and ST107B), Jiama (ET023) and Linzhi (T016), with their coordinates being given in Table 2. Inset denotes the topography and major active fault zones in Tibet and surrounding regions (after Lee et al., 2003). The white arrows from east Tibet to Yunnan indicate the direction of lower crustal flow. BNS: Bangong-Nujiang suture; ITS: Indus-Tsangpo suture; MCT: Main Central Thrust; STDS: South Tibet Detachment System.

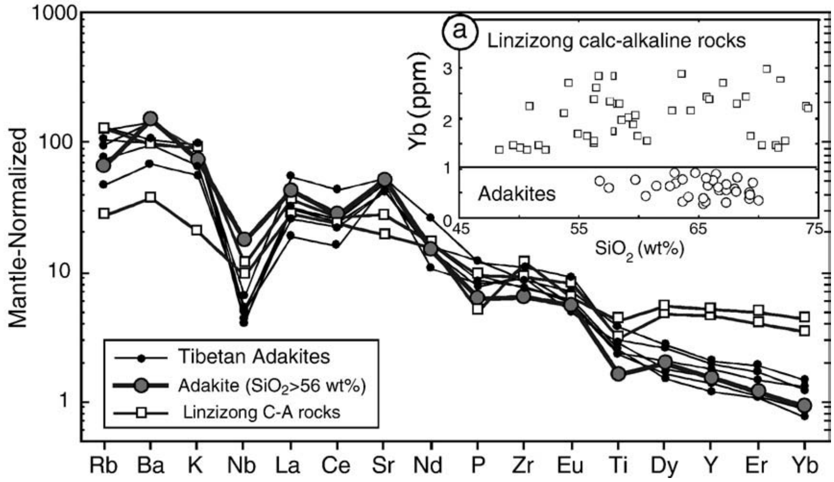

Fig. 2. Primitive mantle-normalized element variation diagram and plots of Yb vs. SiO_2 (inset). Data sources include: Chung et al. (2003, submitted for publication) and Guo et al. (2007) for the southern Tibetan adakites and Lee (2007) and Lee et al. (this volume) for the Paleogene Linzizong calc-alkaline volcanic rocks. The adakite ($SiO_2 > 56$ wt.%), i.e., "average" composition of global adakites (Martin, 1999), is plotted for comparison.

Asia, proposed an Early Miocene slab breakoff beneath southern Tibet for generating the adakites. Nonetheless, this model did not accommodate the observations that the adakitic magmatism began as early as ca. 30 Ma following the Gangdese peak activities at ca. 50 Ma and a magmatic quiescence during ca. 45–30 Ma (see below).

3. Samples and analytical methods

To explore the long-lasting debate on the mechanism responsible for the Tibetan crustal thickening, we conducted in-situ analyses of U–Pb and Hf isotope ratios for zircon separates from the postcollisional

Table 1
Zircon U–Pb age data for postcollisional adakites, southern Tibet.

Spot	U (ppm)	Th (ppm)	Th/U	f_{206} (%)	$^{206}Pb^*/^{238}U \pm 1\sigma$ (%)		$^{207}Pb^*/^{235}U \pm 1\sigma$ (%)		Error corr.	$^{206}Pb^*/^{238}U$ Age ($Ma \pm 1\sigma$)	
T060B											
T060b-01	499	404	0.81	9.42	0.00230	2.2	0.0086	51	0.0424	14.8	0.5
T060b-03	793	902	1.14	5.16	0.00241	1.9	0.0131	20	0.0968	15.5	0.4
T060b-04	587	609	1.04	10.74	0.00219	2.1	0.0072	55	0.0375	14.1	0.5
T060b-05	466	378	0.81	7.45	0.00236	2.2	0.0155	22	0.1027	15.2	0.5
T060b-06	359	309	0.86	62.54	0.00238	3.9	−0.0107	129	−0.0302	15.3	3.9
T060b-09	478	457	0.96	5.36	0.00231	2.2	0.0120	12	0.1833	14.9	0.4
T060b-10	598	551	0.92	5.11	0.00232	2.1	0.0116	15	0.1360	14.9	0.4
T060b-11	550	502	0.91	5.04	0.00238	2.1	0.0145	13	0.1642	15.3	0.4
T060b-12	502	464	0.92	4.04	0.00241	2.1	0.0149	20	0.1072	15.5	0.4
Weighted mean (2σ)										15.1	0.3
T060b-02	735	554	0.75	6.49	0.00323	1.8	0.0147	24	0.0756	20.8	0.5
T060b-07	352	205	0.58	4.48	0.00641	1.8	0.0401	13	0.1394	41.2	0.9
T060b-08	969	256	0.26	1.66	0.00462	1.6	0.0294	5	0.3240	29.7	0.5
ST107A											
ST107a-01.1	1342	483	0.36	1.37	0.00457	2.4	0.0277	6	0.3725	29.4	0.8
ST107a-01.2	401	226	0.56	6.94	0.00446	2.2	0.0328	25	0.0859	28.7	0.9
ST107a-02	541	311	0.57	6.64	0.00463	2.1	0.0236	28	0.0745	29.8	0.8
ST107a-03	1750	580	0.33	1.82	0.00488	1.8	0.0296	4	0.5088	31.4	0.6
ST107a-04	1617	862	0.53	1.36	0.00476	1.8	0.0319	8	0.2207	30.6	0.6
ST107a-05	2691	1006	0.37	0.93	0.00476	1.7	0.0313	5	0.3494	30.6	0.6
ST107a-06	2603	1569	0.60	1.66	0.00468	1.7	0.0280	5	0.3355	30.1	0.6
ST107a-07	3213	6916	2.15	15.69	0.00503	1.7	−0.0186	9	−0.1862	32.3	1.5
ST107a-08	1604	1094	0.68	2.03	0.00467	1.8	0.0263	4	0.4205	30.0	0.6
Weighted mean (2σ)										30.3	0.6
ST107B											
ST107b-01	1625	513	0.32	2.46	0.00476	0.8	0.0280	6	0.1240	30.6	0.3
ST107b-02	1833	2911	1.59	4.22	0.00453	0.8	0.0151	9	0.0867	29.1	0.4
ST107b-03	3020	1472	0.49	1.70	0.00477	0.7	0.0297	2	0.3309	30.6	0.3
ST107b-05	2302	917	0.40	0.80	0.00490	0.7	0.0336	4	0.2037	31.5	0.2
ST107b-06	465	244	0.52	5.20	0.00458	1.4	0.0247	12	0.1130	29.5	0.5
ST107b-07	1603	666	0.42	1.63	0.00491	1.2	0.0292	3	0.3451	31.6	0.4
ST107b-08	2052	503	0.25	1.16	0.00488	0.8	0.0305	3	0.2878	31.4	0.3
ST107b-09	2327	3470	1.49	3.24	0.00496	0.8	0.0193	4	0.1770	31.9	0.4
ST107b-10	2501	3178	1.27	4.59	0.00483	0.7	0.0108	11	0.0668	31.0	0.4
ST107b-11	1906	1795	0.94	1.59	0.00483	0.8	0.0308	4	0.1920	31.1	0.3
weighted mean (2σ)										31.0	0.5
ST107b-04	1364	557	0.41	2.78	0.00550	0.8	0.0294	9	0.0908	35.4	0.4

Table 2
In-situ U–Pb ages and Hf isotopes of zircon separates from postcollisional adakites, southern Tibet.

Sample	Grain		U (ppm)	Th (ppm)	Th/U	age (Ma)[a]	±2σ	$^{176}Lu/^{177}Hf$	±2σ	$^{176}Yb/^{177}Hf$	±2σ	$^{176}Hf/^{177}Hf$	±2σ	εHf(T)	T_{DM} (Ma)	T^{C}_{DM} (Ma)
T060B	T060b-01		499	404	0.81	14.78	1.04	0.000498	0.000022	0.01055	0.00056	0.282876	0.000026	4.0	509	815
90.04°E	T060b-02		735	554	0.75	20.82	1.1	0.000443	0.000011	0.00993	0.00028	0.282989	0.000030	8.1	355	563
29.52°N	T060b-03		793	902	1.14	15.52	0.86	0.000535	0.000044	0.01137	0.00126	0.282888	0.000030	4.4	493	788
4050 m	T060b-04		587	609	1.04	14.11	1.	0.000525	0.000032	0.01122	0.00086	0.282904	0.000040	5.0	471	754
	T060b-05		466	378	0.81	15.17	0.92	0.000417	0.000012	0.00865	0.00022	0.282861	0.000024	3.5	528	848
	T060b-06		359	309	0.86	15.3	7.8	0.000403	0.000011	0.00896	0.00022	0.282832	0.000030	2.5	567	911
	T060b-07		352	205	0.58	41.16	1.86	0.000742	0.000220	0.02106	0.00600	0.282744	0.000034	−0.1	692	1088
	T060b-08		969	256	0.26	29.73	1.02	0.000198	0.000022	0.00413	0.00048	0.282922	0.000032	6.0	443	704
	T060b-09		478	457	0.96	14.87	0.9	0.000540	0.000022	0.01170	0.00052	0.282898	0.000030	4.8	480	767
	T060b-10		598	551	0.92	14.92	0.84	0.000527	0.000005	0.01099	0.00016	0.282930	0.000032	5.9	436	696
	T060b-11		550	502	0.91	15.31	0.88	0.000478	0.000026	0.00958	0.00058	0.282870	0.000034	3.8	517	828
	T060b-12		502	464	0.92	15.5	0.88	0.000467	0.000014	0.00959	0.00028	0.282913	0.000028	5.3	458	733
ET023	ET023-01	c	3540	2876	0.81	18.08	0.5	0.000852	0.000030	0.01751	0.00088	0.283030	0.000026	9.5	303	475
91.60°E	ET023-01	r						0.000599	0.000011	0.01211	0.00028	0.283064	0.000042	10.7[b]	254	400
29.61°N	ET023-02		724	264	0.36	18.72	0.72	0.000571	0.000026	0.01070	0.00034	0.283010	0.000022	8.8	328	518
5121 m	ET023-03		456	192	0.42	16.56	0.78	0.000620	0.000012	0.01116	0.00016	0.283006	0.000022	8.6	334	528
	ET023-04		310	115	0.37	17.31	0.72	0.000590	0.000008	0.01103	0.00013	0.282989	0.000019	8.1	356	565
	ET023-05	c	404	204	0.5	17.24	0.8	0.000651	0.000005	0.01308	0.00014	0.283037	0.000028	9.8	292	460
	ET023-05	r						0.000649	0.000038	0.01380	0.00086	0.282956	0.000046	6.9[b]	402	638
	ET023-06		371	189	0.51	16.64	0.82	0.000415	0.000020	0.00860	0.00044	0.282986	0.000034	7.9	359	572
	ET023-07		323	130	0.4	17.25	1.04	0.000536	0.000026	0.01085	0.00058	0.282994	0.000028	8.2	349	554
	ET023-08		636	328	0.52	16.95	0.78	0.000647	0.000022	0.01193	0.00036	0.283052	0.000024	10.3	271	427
	ET023-09		242	134	0.55	15.09	0.62	0.000457	0.000026	0.00994	0.00050	0.283020	0.000030	9.1	313	498
	ET023-10		391	166	0.42	16.43	0.74	0.000607	0.000018	0.01219	0.00020	0.283025	0.000032	9.3	308	487
	ET023-11.1		396	210	0.53	16.02	1.04	0.000427	0.000015	0.00982	0.00030	0.283021	0.000030	9.2	312	496
	ET023-11.2		327	118	0.36	16.3	0.66	0.000599	0.000022	0.01199	0.00056	0.283038	0.000028	9.8	290	458
	ET023-12.C	c	1329	813	0.61	132.8	3.4	0.001837	0.000140	0.04851	0.00320	0.282934	0.000022	8.6	446	622
	ET023-12.C	r						0.003029	0.000240	0.07346	0.00600	0.282827	0.000030			
	ET023-12.R		218	98	0.45	15.24	1.38	0.000521	0.000013	0.01229	0.00044	0.283108	0.000028	12.2	194	304
T016	T016-01.1	c	292	173	0.59	63.49	1.96	0.000458	0.000002	0.01231	0.00005	0.282430	0.000028	−10.7	1108	1757
94.58°E	T016-01.1	r						0.000552	0.000020	0.01441	0.00052	0.282499	0.000048	−8.2[b]	1018	1607
29.57°N	T016-01.2	c	440	37	0.08	64.04	1.86	0.000394	0.000004	0.00972	0.00011	0.282593	0.000028	−4.9	888	1402
3976 m	T016-01.2	r						0.000366	0.000003	0.00876	0.00007	0.282636	0.000032	−3.4[b]	830	1309
	T016-02	c	972	166	0.17	46.64	1.48	0.000277	0.000005	0.00774	0.00009	0.282880	0.000032	4.9	500	786
	T016-02	r						0.000245	0.000004	0.00740	0.00011	0.282826	0.000040	3.0[b]	573	904
	T016-03		400	112	0.28	587.6	9.2	0.000286	0.000022	0.00747	0.00060	0.282561	0.000026	5.8	928	1142
	T016-04		769	344	0.45	52.3	1.1	0.001182	0.000026	0.02783	0.00066	0.282846	0.000028	3.8	559	859
	T016-05		358	20	0.06	24.55	1.64	0.000530	0.000040	0.01338	0.00104	0.282828	0.000036	2.5	574	914
	T016-06		104	69	0.67	22.4	2.8	0.000723	0.000060	0.01839	0.00150	0.282886	0.000026	4.5	498	788
	T016-07		262	174	0.66	25.92	1.12	0.001188	0.000032	0.03294	0.00102	0.282860	0.000028	3.7	540	844
	T016-08	c	981	823	0.84	27.2	0.82	0.001223	0.000013	0.03465	0.00040	0.282761	0.000026	0.2	677	1060
	T016-08	r						0.001384	0.000052	0.03829	0.00146	0.282846	0.000030	3.2[b]	562	874
	T016-09.C	c	45	41	0.92	1143.	52.	0.000421	0.000003	0.01087	0.00012	0.282123	0.000030	2.9	1515	1747
	T016-09.C	r						0.000474	0.000026	0.01157	0.00050	0.282172	0.000050	4.6[b]	1452	1644
	T016-09.R		575	302	0.53	26.83	0.96	0.000493	0.000014	0.01344	0.00036	0.282792	0.000028	1.3	622	991
	T016-11		640	162	0.25	26.62	0.96	0.001306	0.000064	0.03694	0.00170	0.282800	0.000032	1.6	625	975
	T016-12	c	313	335	1.07	1159.	30.	0.000922	0.000012	0.02541	0.00038	0.282083	0.000030	1.5	1589	1847
	T016-12	r						0.000657	0.000032	0.01729	0.00086	0.282185	0.000032			
	T016-13		221	73	0.33	24.02	1.32	0.000739	0.000060	0.01938	0.00172	0.282785	0.000030	1.0	636	1009
	T016-14		61	25	0.41	240.1	14.8	0.000441	0.000008	0.00861	0.00014	0.282742	0.000030	4.3	689	968
	T016-15		124	84	0.68	1198.	44.	0.000498	0.000015	0.01267	0.00030	0.282076	0.000026	2.4	1581	1818
	T016-19.C	c	500	156	0.31	369.4	15.	0.000646	0.000009	0.01591	0.00026	0.282385	0.000020	−5.5	1174	1667
	T016-19.C	r						0.000668	0.000030	0.01680	0.00082	0.282615	0.000046			
	T016-19.M	c	700	171	0.24	59.47	1.74	0.000970	0.000034	0.02648	0.00110	0.282634	0.000030	−3.6	846	1317
	T016-19.M	r						0.000806	0.000020	0.02063	0.00064	0.282573	0.000054	−5.7[b]	925	1450

	T016-19.R		376	101	0.27	26.29	0.88	0.000806	0.000028	0.02166	0.00082	0.282852	0.000028	3.4	546	861
	T016-20	c	2100	993	0.47	27.26	1.16	0.001042	0.000044	0.02908	0.00106	0.282827	0.000030	2.5	583	915
	T016-20	r						0.001188	0.000050	0.03263	0.00150	0.282905	0.000046	5.3[b]	478	744
	T016-21	c	296	95	0.32	24.77	1.62	0.000358	0.000005	0.00965	0.00015	0.282827	0.000038	2.5	573	916
	T016-21	r						0.000454	0.000026	0.01204	0.00066	0.282873	0.000046	4.1[b]	512	815
	T016-22	c	1473	450	0.31	26.11	1.1	0.001478	0.000040	0.04130	0.00106	0.282789	0.000034	1.2	643	999
	T016-22	r						0.001193	0.000136	0.03270	0.00380	0.282850	0.000066	3.3[b]	554	866
	T016-23		384	146	0.38	25.41	1.36	0.001296	0.000102	0.03611	0.00300	0.282751	0.000052	−0.2	692	1083
	T016-24		717	261	0.36	25.48	1.26	0.001266	0.000148	0.03603	0.00460	0.282877	0.000086	4.3	518	807
	T016-27	c	143	23	0.16	29.8	2.2	0.000294	0.000005	0.00762	0.00014	0.282801	0.000038	1.7	607	970
	T016-27	r						0.000289	0.000008	0.00746	0.00017	0.282708	0.000044	−1.6[b]	732	1173
	T016-28		454	198	0.44	2377.6	11.4	0.000601	0.000044	0.01693	0.00136	0.281300	0.000040	2.1	2606	2747
	T016-29		368	162	0.44	25.52	1.56	0.001227	0.000196	0.03418	0.00540	0.282785	0.000028	1.0	644	1008
ST107A	ST107a-1.1	c	1342	483	0.36	29.36	1.52	0.000549	0.000064	0.01312	0.00166	0.282881	0.000038	4.5	503	795
91.89°E	ST107a-1.1	r						0.000350	0.000015	0.00755	0.00044	0.282988	0.000060	8.3[b]	356	560
29.27°N	ST107a-1.2	c	401	226	0.56	28.67	1.78	0.000411	0.000006	0.01041	0.00022	0.282831	0.000034	2.7	568	905
3563 m	ST107a-1.2	r						0.000403	0.000020	0.00967	0.00050	0.282917	0.000058	5.8[b]	452	716
	ST107a-2		541	311	0.57	29.78	1.6	0.000376	0.000012	0.00915	0.00044	0.282862	0.000038	3.9	526	836
	ST107a-3		1750	580	0.33	31.4	1.24	0.000809	0.000036	0.01824	0.00120	0.282830	0.000028	2.7	576	906
	ST107a-4		1617	862	0.53	30.63	1.26	0.000683	0.000020	0.01664	0.00054	0.282856	0.000019	3.7	538	849
	ST107a-5		2691	1006	0.37	30.64	1.14	0.000957	0.000026	0.02019	0.00064	0.282915	0.000032	5.7	462	720
	ST107a-6		2603	1569	0.6	30.12	1.2	0.000809	0.000074	0.01970	0.00186	0.283010	0.000040	9.1	330	511
	ST107a-7		3213	6916	2.15	32.3	3.	0.000366	0.000052	0.00930	0.00178	0.282928	0.000026	6.2	437	690
	ST107a-8		1604	1094	0.68	30.01	1.26	0.000873	0.000052	0.01975	0.00160	0.282910	0.000028	5.5	467	731
ST107B	ST107b-01		1625	513	0.32	30.59	0.62	0.000512	0.000024	0.01097	0.00032	0.282862	0.000024	3.9	528	836
91.89°E	ST107b-02		1833	2911	1.59	29.12	0.82	0.001267	0.000052	0.03378	0.00158	0.283020	0.000030	9.4	320	491
29.27°N	ST107b-03		3020	1472	0.49	30.64	0.52	0.000811	0.000050	0.01733	0.00144	0.282894	0.000028	5.0	488	766
3563 m	ST107b-04		1364	557	0.41	35.37	0.72	0.000889	0.000054	0.02204	0.00130	0.282894	0.000034	5.1	489	763
	ST107b-05		2302	917	0.4	31.5	0.5	0.000500	0.000022	0.01033	0.00046	0.282990	0.000028	8.4	354	554
	ST107b-06		465	244	0.52	29.45	1.06	0.000350	0.000006	0.00809	0.00022	0.282805	0.000032	1.8	602	961
	ST107b-07		1603	666	0.42	31.57	0.8	0.000420	0.000004	0.00895	0.00014	0.282888	0.000028	4.8	492	778
	ST107b-08		2052	503	0.25	31.41	0.52	0.000823	0.000019	0.01743	0.00038	0.282901	0.000028	5.3	479	750
	ST107b-09		2327	3470	1.49	31.92	0.82	0.000408	0.000032	0.00957	0.00108	0.282877	0.000030	4.4	506	802
	ST107b-10		2501	3178	1.27	31.04	0.74	0.000630	0.000036	0.01495	0.00090	0.282947	0.000036	6.9	414	649
	ST107b-11		1906	1795	0.94	31.07	0.62	0.000455	0.000028	0.01144	0.00102	0.282956	0.000036	7.2	400	629

Analytical methods:

1) U–Pb zircon dating was conducted using a SHRIMP II ion microprobe installed in the Institute of Geology, the Chinese Academy of Geological Sciences, Beijing. Zircon grains, together with a zircon U–Pb standard, were cast in an epoxy mount, which was then polished to section the crystals for analysis. Zircons were documented with transmitted and reflected light micrographs and cathodoluminescence images, and the mount was vacuum-coated with a 500 nm layer of high-purity gold. Measurements of U, Th, and Pb, U–Th–Pb ratios and absolute abundances were determined relative to the TEM standard zircon ($^{206}Pb/^{238}U = 0.0668$, corresponding to 417 Ma), analyses of which were interspersed with those of unknown grains, using operating and data processing procedures similar to those established in the RSES, Australian National University. The mass resolution used to measure Pb/Pb and Pb/U isotopic ratios was about 5000 during the analyses. Measured compositions were corrected for common Pb using non-radiogenic ^{204}Pb.

2) *In-situ* Hf isotope analyses were done with a Merchantek LUV213 nm laser ablation microprobe, attached to a Nu plasma multicollector ICP-MS in GEMOC, Macquarie University, Sydney. The analytical procedures and the precision/accuracy of the method were described in detail by Griffin et al. (2000, 2002). The constants and parameters used for relevant Hf isotope calculations are as follows:

$\lambda_{Lu} = 1.93 \times 10^{-11} y^{-1}$

$\varepsilon Hf(T) = [(^{176}Hf/^{177}Hf)^{T}_{Sample}/(^{176}Hf/^{177}Hf)^{T}_{CHUR} - 1] \times 10^4$

$\varepsilon Hf(T) = \{[((^{176}Hf/^{177}Hf)^{0}_{Sample} - (^{176}Lu/^{177}Hf)^{0}_{Sample} \times (e^{\lambda T} - 1))/((^{176}Hf/^{177}Hf)^{0}_{CHUR} - (^{176}Lu/^{177}Hf)^{0}_{CHUR} \times (e^{\lambda T} - 1)) - 1\} \times 10^4$

$T_{DM} = 1/\lambda \times \ln\{1 + [((^{176}Hf/^{177}Hf)^{0}_{Sample} - (^{176}Hf/^{177}Hf)^{0}_{DM})/((^{176}Lu/^{177}Hf)^{0}_{Sample} - (^{176}Lu/^{177}Hf)^{0}_{DM})]\}$

$T^{C}_{DM} = T_{DM} - (T_{DM} - t) \times [(f_{MC} - f_{Sample})/(f_{MC} - f_{DM})]$

$f_{Lu/Hf} = [(^{176}Lu/^{177}Hf)_{Source}/(^{176}Lu/^{177}Hf)_{CHUR,\ 0}] - 1$

$f_{MC} = (0.015/0.0332) - 1 = -0.5482$

$f_{DM} = (0.0384/0.0332) - 1 = 0.1566$

$(^{176}Lu/^{177}Hf)_{CHUR,\ 0} = 0.0332 \pm 2$ (Blichert-Toft and Albarède, 1997)

$(^{176}Hf/^{177}Hf)_{CHUR,\ 0} = 0.282772 \pm 29$ (Blichert-Toft and Albarède, 1997)

$(^{176}Lu/^{177}Hf)_{DM} = 0.0384$

$(^{176}Hf/^{177}Hf)_{DM} = 0.28325$

$(^{176}Lu/^{177}Hf)_{Mean\ Crust} = 0.015$

[a] Magmatic zircons are in black and inherited zircons in red; For zircons <1000 and >1000 Ma, $^{206}Pb^{*}/^{238}U$ ages and $^{207}Pb^{*}/^{206}Pb^{*}$ ages are listed, respectively. (U–Pb age data for magmatic zircons in ET023 and T016 are from Chung et al., 2003).

[b] Age of the core was used in the calculation of the initial Hf isotope value.

adakites and Gangdese batholiths; the latter is part of an ongoing investigation on the Transhimalayan magmatic evolution (Chiu et al., this volume; Lee et al., this volume; Chu et al., 2006; Lee et al., 2007; Liang et al., 2008; Wen et al., 2008a,b; Ji et al., 2009; Chung et al., submitted for publication; Chu et al., submitted for publication). In the Gangdese batholith, we have obtained zircon U–Pb ages for 73 samples coupled with a total of 800+ analyses of zircon Hf isotope data that serve as key information for understanding the petrogenesis and tectonic setting (Chu et al., 2006; Wen et al., 2008b; Ji et al., 2009; Chu et al., submitted for publication).

For the postcollisional adakites, a total of 84 zircons selected from five adakitic samples (Fig. 1) were subjected to Hf isotopic measurements using laser ablation microprobe-multiple collector-inductively coupled plasma mass spectrometry (LAM-MC-ICPMS) at the GEMOC, Macquarie University (Griffin et al., 2002). The $^{176}Hf/^{177}Hf$ ratio obtained for zircon standard Harvard 91500 during the data acquisition is 0.282307 ± 58 (2 standard deviations). The five adakitic samples, including two (ET023 and T016) reported in Chung et al. (2003), were dated using a sensitive high-resolution ion microprobe (SHRIMP) at the Chinese Academy of Geological Sciences, Beijing. Most of the zircons are co-magmatic in origin, except those in sample T016 from the Linzhi area (Fig. 1), in which abundant inherited zircons with a wide range of U–Pb ages from ca. 30 to 2378 Ma are present (see below for more detailed discussions). The analytical procedures were same as those described in Chung et al. (2003) and Chu et al. (2006).

4. Analytical results

The analytical results of zircon U–Pb ages and Hf isotopes are summarized in Tables 1 and 2, respectively. The εHf(T) values, which show the per mil differences of $^{176}Hf/^{177}Hf$ ratios between the sample and chondritic reservoir at the time of zircon crystallization, were calculated using the ^{176}Lu–^{176}Hf decay constant of $1.93 \times 10^{-11} y^{-1}$ reported in Blichert-Toft and Albarède (1997). The conclusions here would not be affected significantly when the alternative decay constants postulated by more recent studies (e.g., Scherer et al., 2001; Bizzarro et al., 2003) are used. For each zircon, we further calculated the Hf isotope "crustal" model age (T^{C}_{DM}), by assuming its parental magma to have been derived from an average continental crust, with $^{176}Lu/^{177}Hf = 0.015$, that originated from the depleted mantle source (Griffin et al., 2002).

4.1. Zircon U–Pb ages

Given that precise age measurements using $^{207}Pb/^{235}U$ and $^{207}Pb/^{206}Pb$ ratios in SHRIMP analysis are feasible usually only for Precambrian zircons, due largely to the fact that ^{235}U now comprises less than 1% of natural U and relatively little ^{207}Pb can be produced in the Phanerozoic (cf. Ireland and Williams, 2003), the weighted means of pooled $^{206}Pb/^{238}U$ ages are taken in this study to represent crystallization ages. Three new adakite samples (T060B, ST107A and ST107B) yielded $^{206}Pb/^{238}U$ ages of 15.1 ± 0.3, 30.3 ± 0.5 and 31.0 ± 0.5 (2σ) Ma, respectively (Table 1 and Fig. 3). Although the measured U and Th concentrations are highly variable, ranging from 359 to 3213 and from 226 to 6919 ppm, respectively, they correlate with each other in general thus yielding Th/U ratios from ~0.3 to 2.2 in accordance with those of igneous zircons (Belousova et al., 2002; Hoskin and Schaltegger, 2003). Only four grains of inherited zircons that show slightly older U–Pb ages than associated co-magmatic zircons were observed (Table 1). The two samples (ST107A and ST107B) collected from the Yaja granodiorite in Zedong area (Fig. 1) yielded coeval zircon ages of ca. 30 Ma, confirming the results by Harrison et al. (2000) and representing the oldest ages obtained for the adakites in southern Tibet. This further supports the argument by Chung et al. (2005) that postcollisonal magmatism started since as early as ca. 30 Ma in the region.

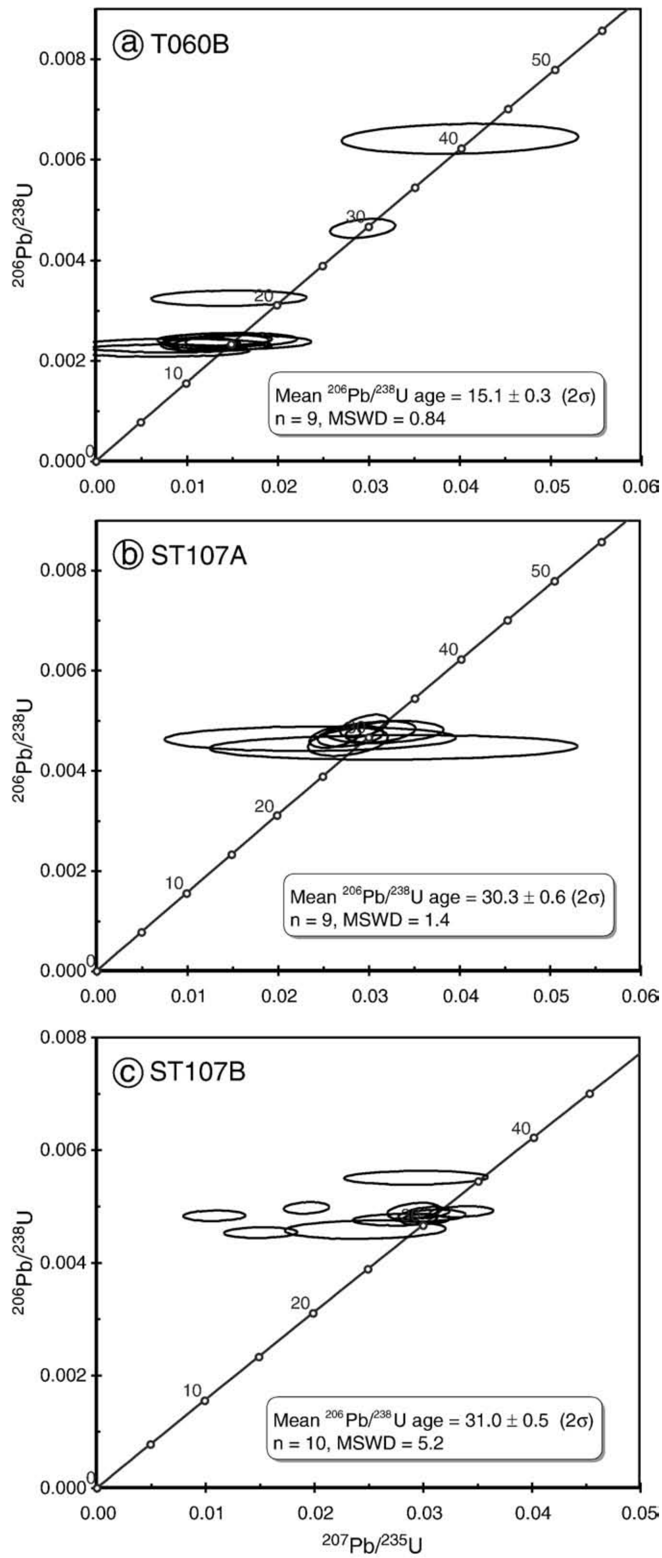

Fig. 3. Zircon U–Pb concordia diagrams of three adakite samples from southern Tibet: (a) T60B, (b) ST107A and (c) ST107B. The $^{206}Pb/^{238}U$ ages are reported with analytical uncertainties at two-standard deviation (2σ) or 95% confidence level.

The other two samples (ET023 and T016) dated by Chung et al. (2003) gave $^{206}Pb/^{238}U$ ages of 17.0 ± 0.5 and 26.2 ± 0.6 (2σ) Ma, respectively. In the latter sample, there are abundant inherited zircons aged variably from ca. 30 to 2378 Ma (Table 2). Additionally, Chung et al. (2003) reported a zircon U–Pb age of 15.0 ± 0.4 Ma for another adakite

Please cite this article as: Chung, S.-L., et al., The nature and timing of crustal thickening in Southern Tibet: Geochemical and zircon Hf isotopic constraints from postcollisional adakites, Tectonophysics (2009), doi:10.1016/j.tecto.2009.08.008

body from Jiama area, close to the sample locality of ET023 (Fig. 1). Hou et al. (2004) reported three zircon U–Pb ages (ca. 18–15 Ma) for an adakitic intrusion from Qulong (near Jiama) and two others from Chongjiang (near Majiang), southern Tibet. Booth et al. (2004), in a zircon U–Pb chonology study around the Namche Barwa area, reported an age of ca. 26 Ma for a "Gangdese granite" (BT4-01) from Linzhi. This sample actually has adakitic geochemical features (high Sr and low Y) and should be correlated to our sample T016 from the same area. These zircon U–Pb age data, together with Ar–Ar and K–Ar age information (Chung et al., 2003; Guo et al., 2007; King et al., 2007; Aitchison et al., 2009), delineate postcollisional adakite magmatism from ca. 30 to 9 Ma in the Lhasa terrane, synchronous to the ultrapotassic/potassic magmatism in the region (ca. 25-10 Ma: Chung et al., 2003, 2005; Guo et al., 2007) and the emplacement of leucogranites in Himalayas (ca. 30-10 Ma: Searle et al., 2003; Zhang et al., 2004a).

4.2. Zircon Hf isotopes

Zircon Hf isotope data are shown by plotting εHf(T) values vs. U–Pb ages of individual analysis (Fig. 4a), and histograms of their Hf crustal model ages (Fig. 4b). All the magmatic zircons of the Tibetan adakites have positive εHf(T) values from +12 to 0 (Table 2). Except those in sample ST107B, magmatic zircons in each sample display rather limited variations in their overall εHf(T) values, smaller than the 2σ external analytical error or "reproducibility" of the method, i.e., ± 3 εHf units (Griffin et al., 2000). The larger εHf(T) variation, from +9.4 to +1.8,

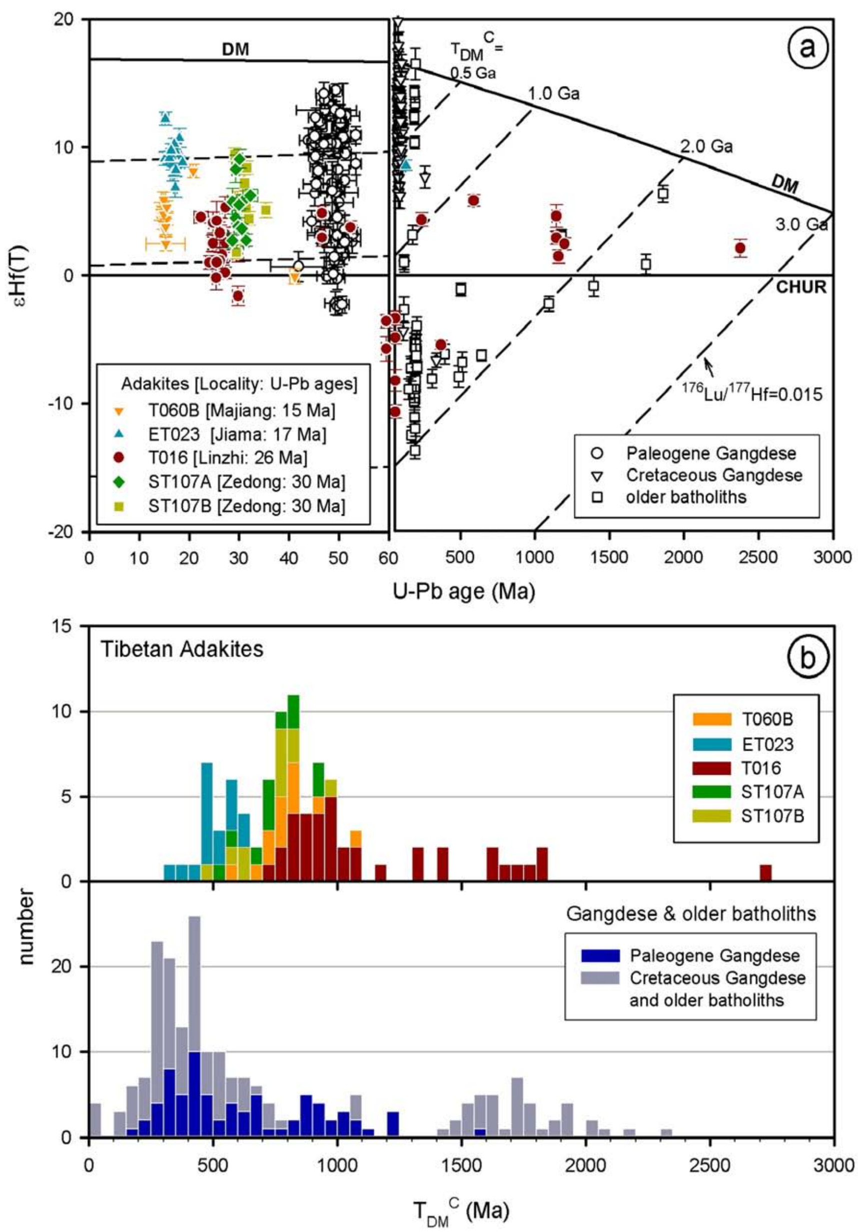

Fig. 4. (a) Plots of initial epsilon Hf isotope values vs. U–Pb ages of zircons studied, and (b) histograms of their Hf crustal model ages (T_{DM}^{C}). In (a), 2σ error bars of individual analyses are shown if larger than symbols, otherwise the analytical errors are smaller than the symbols. Analytical results and further detail of the Tibetan adakites are given in the Table 2. Data for the Paleogene and Cretaceous Gangdese and older batholiths plotted for comparison are from Chu (2006) and Chu et al. (2006, submitted for publication). DM: Depleted mantle; CHUR: Chondrite uniform reservoir. Judging from the positive yet highly variable εHf(T) values observed in the magmatic zircons in both adakites and Gangdese batholiths, their "crustal" model ages are unlikely reflective of real crustal residence times but rather indicate magma generation by involving two end-member sources, namely, a DM-like juvenile mantle input related to the Neotethyan subduction during the late Cretaceous and Paleogene and an inherited old crustal component that started evolving before ca. 2.0 Ga in the Lhasa terrane.

Please cite this article as: Chung, S.-L., et al., The nature and timing of crustal thickening in Southern Tibet: Geochemical and zircon Hf isotopic constraints from postcollisional adakites, Tectonophysics (2009), doi:10.1016/j.tecto.2009.08.008

between magmatic zircons in sample ST107B may result from crystallization through hybridization of ≥2 magmas with different sources (Griffin et al., 2002). Coupled analyses on core and rim of "bigger" zircon grains, enough at least for two non-overlapping laser shots, do not show significant εHf(T) variations (Table 2). Zircons in sample ST107B, however, are too small to do this experiment. Inherited zircons, mostly from sample T016, generally display lower $^{176}Hf/^{177}Hf$ ratios and thus older crustal model ages (Table 2 and Fig. 4).

5. Discussion

5.1. Whole-rock geochemical constraints

Of particular interest here is the geochemical distinction between the adakites (ca. 30–10 Ma) and the Paleogene (ca. 65–45 Ma) Gangdese granitoids and Linzizong volcanics. The latter consist mainly of mafic to felsic calc-alkaline rocks and represent products of the end phase of northward-facing Neotethyan subduction (Chung et al., 2005, for review). In contrast to the adakitic geochemical features in the spidergram (Fig. 2), the Linzizong volcanic rocks have mantle-normalized trace element distribution patterns similar to those of common arc lavas that are marked by higher HREE abundance and lacking the relative enrichment in Sr. The distinction can be also seen by plotting Yb versus SiO_2 contents (Fig. 2a), in which the Linzizong volcanic rocks always contain higher Yb (~1.5–3 ppm) than the Tibetan adakites (<1 ppm).

Based on the consensus that arc magmatism is generated by decompression melting in the mantle wedge, Plank and Langmuir (1988) noted a correlation between crustal thickness and major element composition of arc basalts. The global correlation between trace element chemistry of arc basalts and Moho depth has been recently formulated by Mantle and Collins (2008), who argued that the best correlation exists for maximum light/heavy REE ratios. This may be best exemplified by the Andean convergent margin, along which good correlations between arc lava's REE and crustal thickness have been well documented (e.g., Hildreth and Moorbath, 1988; Kay et al., 1991; Haschke et al., 2002; Kay and Mpodpzos, 2002). Thus, the higher contents of Y and HREE in the Linzizong samples (Fig. 2a) reflect their origin from melting of the mantle wedge that had a normal or "unthickened" crust above it. Specifically, the crustal thickness can be estimated to be ~35 km using Ce/Y ratios (Mantle and Collins, 2008) or ~30–40 km using La/Yb ratios (cf. Kay and Kay, 2002).

Major and trace element data of the postcollisional adakites have been published and discussed in some detail by previous workers (e.g., Chung et al., 2003; Hou et al., 2004; Guo et al., 2007). However, more information may be obtained by plotting La/Yb ratios versus ages of these adakites together with the Gangdese/Linzizong rocks (Fig. 5), suggesting the former to have been generated with a much thicker crust (≥50–55 km). This is consistent with the estimation based on experimental petrology data (e.g., Rapp et al., 1991) that the adakites may be produced by partial melting of garnet-bearing mafic rocks at depths of ~60–70 km in the lower part of thickened crust (Chung et al., 2003; Guo et al., 2007). In the plots (Fig. 5), there are large ranges in La/Yb ratios and thus the hypothesized crustal thickness during the same time period. This could be owing to complex petrogenetic processes, including magma mixing, crystal fractionation and upper crustal contamination, in addition to partial melting with garnet as residue in the lower crust that has the first-order effect on controlling the REE patterns by holding heavy REE and Y (Kay, 1978; Rapp et al., 1991; Martin, 1999). A direct implication from these trace element constraints is that a significant crustal thickening occurred in southern Tibet during the waning of the Gangdese/Linzizong magmatism (ca. 45 Ma; Chung et al., 2005; Lee et al., 2007; Wen et al., 2008b; Ji et al., 2009; Lee et al., this volume) and the start of the adakitic emplacement (ca. 30–26 Ma; Chung et al., 2005 and this study).

5.2. Zircon Hf isotope constraints

Zircons can effectively preserve the initial $^{176}Hf/^{177}Hf$ ratios of the igneous host rocks, so their Hf isotope composition may be utilized as a geochemical tracer for host rock's origin in the same way as whole-rock Nd isotopes. In fact, in-situ analysis of zircon's Hf isotopic composition has been proven a more sensitive and powerful tool than Nd isotopes for detailed study of petrogenetic processes (Griffin et al., 2002). All the magmatic zircons of the Tibetan adakites exhibit positive εHf(T) values (+12 to 0), corresponding to but more heterogeneous than εHf(T) values of their host rocks (+4.4 to +1.9; Chu et al., submitted for publication), which are higher or more radiogenic than the "expected" values calculated from whole-rock Nd isotope ratios of the adakites [εNd (T) = 0 to −6] (Chu et al., submitted for publication) following the "terrestrial array" of Hf–Nd isotopic correlation (Vervoort et al., 1999). Such an "elevated" Hf isotopic signature, however, is not really unexpected because the region of southern Tibet was situated in an

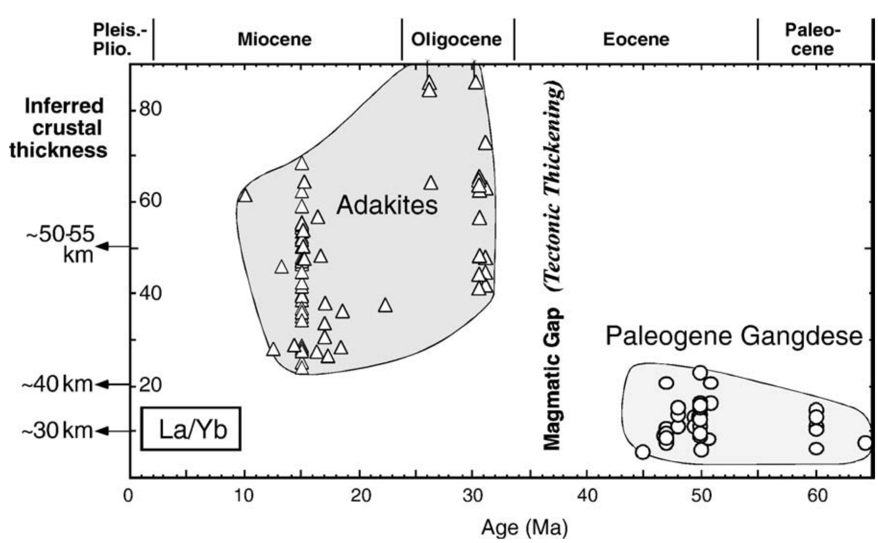

Fig. 5. Plots of La/Yb ratios vs. magmatic ages for the postcollisional adakites and Paleogene Gangdese/Linzizong rocks in southern Tibet, with data from Chung et al. (2003, submitted for publication), Harrison et al. (2000), Hou et al. (2004), Chu et al. (2006), Guo et al. (2007), Lee (2007), Wen (2007), Wen et al. (2008a) and Lee et al. (this volume). The crustal thickness correlation is inferred after Hildreth and Moorbath (1988), Kay et al. (1991, 1994), Haschke et al. (2002) and Kay and Kay (2002), based on the Andean examples. Note the dramatic increase in La/Yb ratios of the rocks produced before/after the magmatic gap during ca. 40–30 Ma, suggesting a major stage of tectonic (and crustal) thickening.

Please cite this article as: Chung, S.-L., et al., The nature and timing of crustal thickening in Southern Tibet: Geochemical and zircon Hf isotopic constraints from postcollisional adakites, Tectonophysics (2009), doi:10.1016/j.tecto.2009.08.008

Andean type convergent margin under which the Neotethyan oceanic slab had been subducting northward until India started colliding with Asia. Our comparative study of the Gangdese batholith (Chu et al., 2006; Ji et al., 2009; Chu et al., submitted for publication) reveals that most Gangdese magmatic zircons have positive εHf(T), with the highest values equal or approximating to the presumed value of the depleted mantle (Fig. 4a). The data, in good agreement with the host rock's Hf isotope ratios [εHf(T) = +13 to +1] (Chu et al., submitted for publication), are also higher than the calculated values from the Nd isotope ratios of the host rocks [εNd(T) = 5 to −3] (Wen, 2007; Wen et al., 2008a). Although detailed petrogenetic discussion of the adakites is beyond the scope of this paper and will be presented together with that of the Gangdese and other Transhimalayan rocks in a separate article (Chu et al., submitted for publication), the highly radiogenic Hf isotopic feature may be attributed to involvement of subducted oceanic sediments (Vervoort et al., 1999; Chauvel et al., 2008) or slab-released aqueous fluids (Pearce et al., 1999; Hanyu and Tatsumi, 2002) that metasomatized the mantle wedge during the Neotethyan subduction. Similar scenarios occur in certain active subduction zones (cf. Chauvel et al., 2008) and have been discussed by Guo et al. (2007) using Sr–Nd–Pb isotope constraints for the adakite petrogenesis.

More importantly, the positive εHf(T) values of all magmatic zircons in the adakites are consistent with a host magma source within the mafic lower crust that is largely juvenile and subduction-related, two prerequisites that also characterize the Gangdese arc magma's source region. Similarities can be also observed in the Hf crustal model age spectra (Fig. 4a–b), in which the adakitic magmatic zircons yield a broad range of relatively young model ages (from ca. 300 to 1100 Ma) overlapping with that of the Paleogene Gangdese zircons. Likewise, the abundant inherited zircons of the Linzhi sample (T016) reveal older U–Pb and Hf model ages, which correspond in general to those of inherited zircons in the Cretaceous Gangdese and older batholiths (Fig. 4a–b), reflecting the existence of early phases of crustal formation in the Lhasa terrane (Chu et al., 2006) and involvement with a certain amount of this old crust component in the magma generation (Chu et al., submitted for publication). We note that the majority of these inherited zircons are from the "older batholiths", which crop out in the Nyainqentanglha range just north of the Gangdese batholith (Chu et al., 2006). These batholiths, consisting mainly of S-type granitoids, are part of the northern plutonic belt in the Lhasa terrane that is marked by a dominant crustal source (cf. Chiu et al., this volume). The Gangdese batholith, which occurs in the southern part of the Lhasa terrane, by contrast, consists overwhelmingly of I-type granitoids that contain rare inherited zircons (Wen et al., 2008b; Ji et al., 2009).

The above correlation between the adakites and Gangdese granitoids regarding zircons' Hf isotopes suggests a genetic link of the source regions between the pre- and postcollisional magmas in southern Tibet, which leads us to infer a juvenile lower crust component resulting from basaltic underplating related to the Neotethyan subduction (see below for detail). This is consistent with the view that the Tibetan crust was thickened by internal deformation, rather than by "exotic" processes such as injection of the Indian crust. Although old (Asian and/or Indian) continental crust may have been involved in producing some adakites (e.g., sample T016), the high Hf isotope ratios observed in all magmatic zircons imply that contamination of the old crust played a less significant or minor role in the generation of adakitic magmas, which were derived largely from the juvenile lower crust source.

5.3. Implications for basaltic underplating and lithospheric weakening

The above data also address the role of intrusion or underplating of basaltic magmas in producing the mafic lower crust of the Lhasa terrane. Recurrent crustal growth from the mantle should have taken place since the Mesoproterozoic, as evidenced by the zircon's U–Pb age and Hf isotope data (Fig. 4). Here we address the last and likely most significant addition by basaltic magma underplating that occurred during the late Cretaceous and mid-Eocene time in association with the Neotethyan subduction. The underplating, and its subsequent remelting, played a crucial role in the generation of the voluminous Gangdese batholith and Linzizong successions, in particular in generating the Paleogene magmatic "flare-ups" at ca. 50 Ma (Lee et al., this volume; Chung et al., 2005; Lee et al., 2007; Wen et al., 2008b). The scenarios could be like those proposed for the California arc (Ducea, 2001; Saleeby et al., 2003), where Mesozoic granitic batholiths shared a principal source that was a polygenetic hydrous lower crust dominated by mantle wedge-derived mafic intrusions. Substantial melting of this lower crust, a required condition for forming the vast batholiths and thick granitic crust there, may have produced a significant residual mass made up of mafic (eclogite) and ultramafic (garnet pyroxenite) lithologies which eventually became a dense root and started foundering with its underlying lithospheric mantle since Mio-Pliocene time (Saleeby et al., 2003; Zandt et al., 2004). We note that similar lithospheric delamination models have also been proposed in the central Andes (Kay et al., 1999; Kay and Mpodpzos, 2001).

In southern Tibet, where was underlain by a thinner crust during emplacement of the Gangdese batholith, the basaltic underplates and their melting residues should have been mostly in the granulite facies. Nevertheless, intense magma underplating and remelting in a continental arc may result in weak (and soft) lower crust and sub-arc mantle, and this weakened structure has a favored rheology for homogeneous pure-shear thickening if continental collision succeeds (cf. Thompson et al., 2001). It is hence postulated that the Paleogene Gangdese/Linzizong magmatic activities gave rise to a thermally weakened lithosphere in the southern Lhasa terrane. Continued northward Indian impingement, consequently, was capable of causing distributed lithospheric thickening in southern Tibet in a rather effective fashion during ca. 45 and 30 Ma at the early stage of the India–Asia collision.

5.4. The nature and timing of crustal thickening

The new observations, combined with the existing constraints synthesized in Chung et al. (2005), lead us to propose the following sequence of tectonomagmatic events to account for the nature and timing of continental crustal thickening in southern Tibet (Fig. 6). This model emphasizes the importance of precollisional geodynamic processes on the initial conditions and evolution of the Himalayan–Tibetan orogenesis. Starting with the Neotethyan subduction that resulted in the Gangdese arc since Cretaceous time, the Lhasa terrane was characterized by a relatively weak deep lithosphere made up of fluid/melt softened lithospheric mantle and abundant mafic intrusions in the lower crust. Geochronologic data (Lee et al., 2007; Wen et al., 2008b; Ji et al., 2009; Lee et al., this volume; and references therein) indicate southward migration and intensification of the arc magmatism in the late Cretaceous (Fig. 5a), suggesting a roll back of the Neotethyan subducting slab that later detached from the adhering and more buoyant Indian continental lithosphere. The slab detachment, which we infer to have occurred at ca. 50 Ma (Fig. 6b), would have not only caused the Paleogene magmatic flare-ups, and thus enhanced thermal softening of the Lhasa lithosphere, but also eliminated slab pull, thus preventing the buoyant Indian cratonic lithosphere from moving further downward. The continued northward push from the colder and stronger Indian plate, then, led to a "hard collision" into the softened Lhasa deep lithosphere and caused significant contraction and thickening of the latter (Fig. 6c).

Consequently, the Gangdese/Linzizong magmatism terminated and an orogenic root was created during an igneous quiescence period of ca. 45–30 Ma in the southern part of the Lhasa terrane (Fig. 6c–d). Provided that the crust was thickened to ≥55 km (Fig. 5), eclogitization of the crustal root, which was originally composed of mafic granulitic rocks, could have been facilitated by the preexisting "wet" condition in the Lhasa lithosphere owing to the protracted Neotethyan subduction; and

Please cite this article as: Chung, S.-L., et al., The nature and timing of crustal thickening in Southern Tibet: Geochemical and zircon Hf isotopic constraints from postcollisional adakites, Tectonophysics (2009), doi:10.1016/j.tecto.2009.08.008

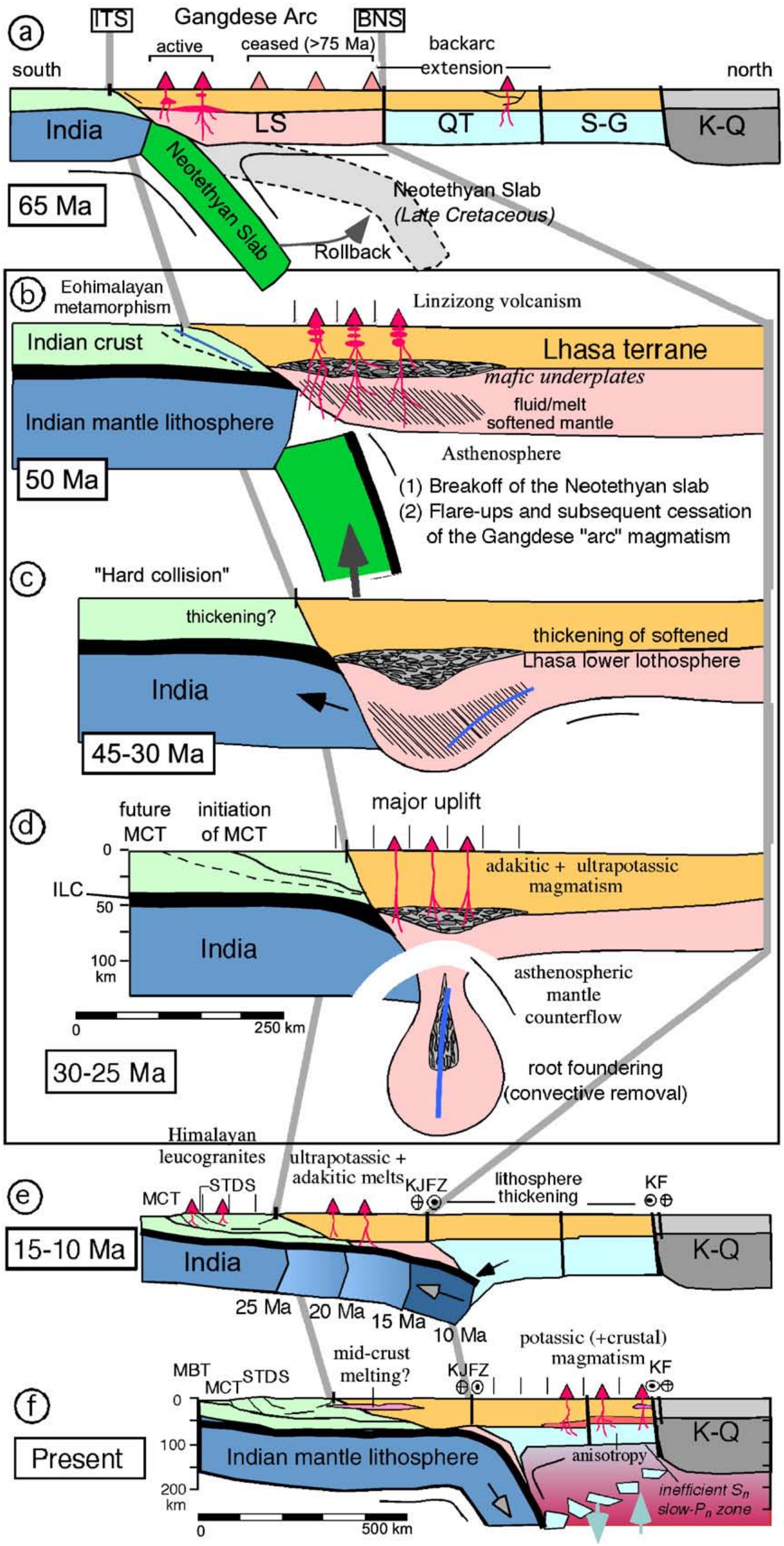

Fig. 6. A sequential history of the Tibetan tectonomagmatic activities illustrated by ~90°E north–south cross sections. Whilst stages (a), (e) and (f) for the entire plateau are taken with slight modification from Chung et al. (2005), those of (b)–(d) depict the major scenarios that we propose for the crustal thickening and orogenic root foundering in southern Tibet. The scale shown in 6d is shared through b to d, while that in 6f is for e and f. The proposed sequence is discussed in the text. More details with referencing can be found in Chung et al. (2005).

partially eclogitized rocks or garnet amphibolites may have also formed via incomplete metamorphic reactions (Chung et al., 2003). This high-density lower crust, with thickened Lhasa lithospheric mantle root, became unstable and began downwelling when the maximum sustainable gravitational potential-energy level had been reached (Fig. 6d). Resultant upward counterflow of the hotter asthenosphere would have greatly raised the geotherm beneath the region and caused partial melting in the remaining lower crust and enriched lithospheric mantle to form adakitic and ultrapotassic magmas, respectively. Under the framework of this hypothesis, the onset of the magmatism during ca. 30–25 Ma in the Oligocene (Fig. 6d) should coincide or slightly postdate the foundering event and be able to constrain the timing that removal of the orogenic root started.

5.5. Broader implications for Tibetan–Himalayan tectonic evolution

The root foundering has additional effects for the Tibetan–Himalayan orogenesis. First, it may have caused a sudden rise in topography to form the southern part of the Tibetan plateau since Oligocene time (cf. Chung et al., 2005). Secondly, it created room that let the Indian cratonic lithospheric mantle, and its overlying mafic lower crust made of dry and unusually strong granulites (Jackson et al., 2004), start thrusting northward under Tibet (Fig. 6d–e). This eventually made it crust among the world's thickest, with an overall (Asian + Indian) crustal thickness reaching to ~70–80 km in southern Tibet (Jackson, 2002; Chen and Yang, 2004). The Indian upper/middle continental crust, by contrast, was too buoyant to have been underthrust together so that was exhumed backward to the south along the Main Central Thrust and the South Tibet Detachment System. Our model, hence, predicts the Himalayan tectonomagmatism and associated southward exhumation of the metamorphic rocks, through the presumed crustal channel flow (Hodges et al., 2001; Beaumont et al., 2001), to have been initiated at ca. 30–25 Ma during Oligocene time. This prediction is in good agreement with the numerical modeling result (e.g., Jamieson et al., 2004) and recent geologic observations (e.g., Searle et al., 2003; Zhang et al., 2004a).

The northward underthrusting of the Indian plate (Fig. 6e), which could have taken place only after the orogenic root's removal, exerted key controls to the Tibetan tectonic evolution. It may have not only terminated the adakitic and ultrapotassic magmatism by shutting off the heat from the asthenosphere (Chung et al., 2003), but offered support that holds up the high topography of the southern Tibetan plateau (Owens and Zandt, 1997). Hence, even though the region should have had gravitational collapse after a topographic uplift caused by the root foundering, its altitude has remained unchanged over at least the past 15 m.y. (Spicer et al., 2003). This underthrusting, furthermore, largely deformed and pushed the remaining Lhasa lithospheric mantle northward, and thus squeezed the Qiangtang and Songpan-Ganze terranes where a thin and thermally softened lithosphere was existing as a result of Paleogene back-arc extension with associated magmatism (Chung et al., 2005). The squeezing lasted and eventually led to formation of the northern Tibetan plateau that, however, would have not attained its present elevation and size until the middle Miocene when the thickened lithosphere began destruction from its base by the "hard" contact of the underthrust Indian plate (Fig. 6e–f).

6. Concluding remarks

We propose in southern Tibet that the lithosphere was already hot and soft before the India's hard collision. Therefore, the Tibetan lithosphere underwent distributed pure-shear thickening that later evolved northward and caused diachronous uplift of Tibetan topography. There are systematic temporal–spatial variations in the Tibetan postcollisional magmatism (Chung et al., 2005), which suggest a protracted thermal perturbation in the Tibetan deep lithosphere. The continuous internal deformation observed in modern Tibet (e.g., Wright et al., 2004; Zhang et al., 2004b), thus, may not be ephemeral but more likely represents a general scenario that has been operating throughout the India–Asia collisional history. This study with emphasis on the preexisting lithospheric controls to the Tibetan–Himalayan evolution has broad implications for not only the continental tectonics in Asia but also global orogenesis related to continental or terrane collisions. During terrane assemblages, such as those that formed the Asian continent, foregoing magma processes including underplating and remelting in the lower crust may have served as a common, rather than an occasional, mechanism to effectively soften/weaken the continents involved and thus cause viscous instead of rigid intraplate deformation.

In addition to the favored, pure-shear thickening model presented in Fig. 6, there are other models proposed for crustal thickening in Tibet that may also account for the time series and geochemical features observed in the Tibetan postcollisional magmatism. For example, a number of modeling studies have argued for ductile flow of the softened Tibetan lithosphere (e.g., Royden et al., 1997; Cook and Royden, 2008; and references therein), with the upper crust being mechanically detached from its mantle lithosphere by ductile, non-coaxial crustal flow that occurs within the middle and lower crust. These studies suggested that preexisting variations in crustal strength would have influenced not only the mode of crustal thickening but also the growth of the entire plateau. By contrast, Tapponnier et al. (2001) ascribed crustal thickening and growth of Tibet to a series of northeastward stepping transpressive wedges. We note that this model involves a key argument about the distribution of high-K magmas, which is genetically correlated with the adakites reported in this study, but does not require delamination of Tibetan lithosphere as widely thought. Furthermore detailed investigations on the time-space patterns and geochemical characteristics of the postcollisional magmatism are urgently needed to comprehend our understanding about the relations between the magmatic records and tectonic evolution of the Tibetan plateau.

Acknowledgments

We thank H.-Y. Lee, Q. Qian, Mary Yeh and Q. Zhang for help in the field, B. Song and H. Tao for help with zircon dating experiments, and Bill Griffin for insightful discussion on the Hf isotope data. Critical and constructive comments offered by Sue Kay and two anonymous reviewers, and the guest editor Wang-Ping Chen, were of great help with improving the presentation of the paper. This study benefited from the financial supports by the National Science Council, Taiwan, ROC.

References

Aitchison, J.C., Ali, J.R., Chan, A., Davis, A.M., Lo, C.-H., 2009. Tectonic implications of felsic tuffs within the lower Miocene Gangrinboche conglomerates, southern Tibet. J. Asian Earth Sci. 34, 287–297.

Allegrè, C.J., Courtillot, V., Tapponnier, P., et al., 1984. Structure and evolution of the Himalaya–Tibet orogenic belt. Nature. 307, 17–22.

Beaumont, C., Jamieson, R.A., Nguyen, M.H., Lee, B., 2001. Himalayan tectonics explained by extrusion of a low-viscosity channel coupled to focused surface denudation. Nature. 414, 738–742.

Belousova, E.A., Griffin, W.L., O'Reilly, S.Y., Fisher, M.I., 2002. Igneous zircon: trace element composition as an indicator of source rock type. Contrib. Mineral. Petrol. 143, 602–622.

Bizzarro, M., Baker, J.A., Haack, H., Ulfbeck, D., Rosing, M., 2003. Early history of Earth's crust–mantle system inferred from hafnium isotopes in chondrites. Nature. 421, 931–933.

Blichert-Toft, J., Albarède, F., 1997. The Lu–Hf isotope geochemistry of chondrites and the evolution of the mantle–crust system. Earth Planet. Sci. Lett. 148, 243–258.

Booth, A.L., Zeitler, P.K., Kidd, W.S.F., Wooden, J., Liu, Y., Idleman, B., Hren, M., Chamberlain, C.P., 2004. U–Pb zircon constraints on tectonic evolution of southeastern Tibet, Namche Barwa area. Am. J. Sci. 304, 889–929.

Chauvel, C., Lewin, E., Carpentier, M., Arndt, N.T., Marini, J.-C., 2008. Role of recycled oceanic basalts and sediment in generating the Hf–Nd mantle array. Nat. Geosci. 1, 64–67.

Chemenda, A.I., Burg, J.-P., Mattauer, M., 2000. Evolutionary model of the Himalaya–Tibet system: geopoem based on new modeling, geological and geophysical data. Earth Planet. Sci. Lett. 174, 397–409.

Chen, W.-P., Yang, Z., 2004. Earthquakes beneath the Himalayas and Tibet: evidence for strong lithospheric mantle. Science. 304, 1949–1952.

Chiu, H.-Y., Chung, S.-L., Wu, F.-Y., Liu, D., Liang, Y.-H., Lin, I-J., Iizuka, Y., Xie, L.-W., Wang, Y., Chu, M.-F., this volume. Zircon U-Pb and Hf isotopic constraints from eastern Transhimalayan batholiths on the precollisional magmatic and tectonic evolution in southern Tibet. Tectonophysics.

Chu, M.-F., 2006. Application of ICP-MS to the study of Transhimalayan petrogenesis. Ph.D thesis, National Taiwan University.

Chu, M.-F., Chung, S.-L., Song, B., Liu, D., O'Reilly, S.Y., Pearson, N.J., Ji, J., Wen, D.-J., 2006. Zircon U–Pb and Hf isotope constraints on the Mesozoic tectonics and crustal evolution of southern Tibet. Geology 34, 745–748.

Chu, M.-F., Chung, S.-L., O'Reilly, S.Y., Pearson, N.J., Wu, F.-Y., Li, X.-H., Liu, D., Ji, J., Chu, C.-H., Gallet, S., submitted for publication. Tibetan orogeny with India's hidden inputs revealed by Hf isotopes of Transhimalayan zircons and host rocks.

Chung, S.-L., Liu, D., Ji, J., Chu, M.-F., Lee, H.-Y., Wen, D.-J., Lo, C.-H., Lee, T.-Y., Qian, Q., Zhang, Q., 2003. Adakites from continental collision zones: melting of thickened lower crust beneath southern Tibet. Geology 31, 1021–1024.

Chung, S.-L., Chu, M.-F., Zhang, Y., Xie, Y., Lo, C.-H., Lee, T.-Y., Lan, C.-Y., Li, X.-H., Zhang, Q., Wang, Y., 2005. Tibetan tectonic evolution inferred from spatial and temporal variations in post-collisional magmatism. Earth-Sci. Rev. 68, 173–196.

Chung, S.-L., Shinjo, R., Wu, F.-Y., Chu, C.-H., Gallet, S., Lee, H.-Y., Lo, C.-H., submitted for publication. Postcollisional magmatism in southern Tibet: ages, isotopic characteristics, petrogenesis, and geodynamic significance.

Cook, K.L., Royden, L.H., 2008. The role of crustal strength variations in shaping orogenic plateaus, with application to Tibet. J. Geophys. Res. 113, B08407. doi:10.1029/2007JB005457.

Coulon, C., Maluski, H., Bollinger, C., Wang, S., 1986. Mesozoic and Cenozoic volcanic rocks from central and southern Tibet: ^{39}Ar–^{40}Ar dating, petrological characteristics and geodynamical significance. Earth Planet. Sci. Lett. 79, 281–302.

DeCelles, P., Robinson, D.M., Zandt, G., 2002. Implications of shortening in the Himalayan fold–thrust belt for uplift of the Tibetan plateau. Tectonics 21, 1062. doi:10.1029/2001TC001322.

Defant, M.J., Drummond, M.S., 1990. Derivation of some modern arc magmas by melting of young subducted lithosphere. Nature. 347, 662–666.

Ducea, M.N., 2001. The California arc: thick granitic batholiths, eclogitic residues, lithosphere-scale thrusting, and magmatic flare-ups. GSA Today 11, 4–10.

England, P.C., Houseman, G.A., 1985. Role of lithospheric strength heterogeneities in the tectonics of Tibet and neighbouring regions. Nature. 315, 297–301.

England, P.C., Houseman, G.A., 1989. Extension during continental convergence, with application to the Tibetan plateau. J. Geophys. Res. 94, 17561–17579.

Gao, Y., Hou, Z., Kamber, B.S., Wei, R., Meng, X., Zhao, R., 2007. Adakite-like porphyries from the southern Tibetan continental collision zone: evidence for slab melt metasomatism. Contrib. Mineral. Petrol. 153, 105–120.

Griffin, W.L., Pearson, N.J., Belousova, E., Jackson, S.E., van Achterbergh, E., O'Reilly, S.Y., Shee, S.R., 2000. The Hf isotope composition of cratonic mantle: LAM-MC-ICPMS analysis of zircon megacrysts in kimberlites. Geochim. Cosmochim. Acta 64, 133–147.

Griffin, W.L., Wang, X., Jackson, S.E., Pearson, N.J., O'Reilly, S.Y., Xu, X., Zhou, X., 2002. Zircon chemistry and magma mixing, SE China: in-situ analysis of Hf isotopes, Tonglu and Pingtan igneous complexes. Lithos 61, 237–269.

Guo, Z., Wilson, M., Liu, J., 2007. Post-collisional adakites in south Tibet: products of partial melting of subduction-modified lower crust. Lithos 96, 205–224.

Haines, S.S., Klemperer, S.L., Brown, L., Guo, J., Mechie, J., Meissner, R., Ross, A., Zhao, W., 2003. INDEPTH III seismic data: from surface observations to deep crustal processes in Tibet. Tectonics 22, 1001. doi:10.1029/2001TC001305.

Hanyu, T., Tatsumi, Y., 2002. A contribution of slab-melts to the formation of high-Mg andesite magmas; Hf isotopic evidence from SW Japan. Geophys. Res. Lett. 29, 2051. doi:10.1029/2002GL015856.

Harrison, H.M., Yin, A., Grove, M., Lovera, O.M., 2000. The Zedong window: a record of superposed Tertiary convergence in southeastern Tibet. J. Geophys. Res. 105, 19211–19230.

Haschke, M., Siebel, W., Günther, A., Scheuber, E., 2002. Repeated crustal thickening and recycling during the Andean orogeny in north Chile (21°–26°S). J. Geophys. Res. 107. doi:10.1029/2001JB000328.

Hildreth, W., Moorbath, S., 1988. Crustal contributions to arc magmatism in the Andes of central Chile. Contrib. Mineral. Petrol. 98, 455–489.

Hodges, K.V., Hurtado, J.M., Whipple, K.X., 2001. Southward extrusion of Tibetan crust and its effect on Himalayan tectonics. Tectonics 20, 799–809.

Hoskin, P.W.O., Schaltegger, U., 2003. The composition of zircon and igneous and metamorphic petrogenesis. In: Manchar, J.M., Hoskin, P.W.O. (Eds.), Zircon, Reviews of Mineralogy and Geochemistry, vol. 53, pp. 27–62.

Hou, Z.-Q., Guo, Y.-F., Qu, X.-M., Rui, Z.-Y., Mo, X.-X., 2004. Origin of adakitic intrusives generated during mid-Miocene east–west extension in southern Tibet. Earth Planet. Sci. Lett. 220, 139–155.

Houseman, G.A., Molnar, P., 1997. Gravitational (Rayleigh-Taylor) instability of a layer with non-linear viscosity and convergence thinning of continental lithosphere. Geophys J Int. 128, 125–150.

Ireland, T.R., Williams, I.S., 2003. Considerations in zircon geochronology by SIMS. In: Manchar, J.M., Hoskin, P.W.O. (Eds.), Zircon, Reviews of Mineralogy and Geochemistry, vol. 53, pp. 215–241.

Jackson, J.A., 2002. Strength of the continental lithosphere: time to abandon the jelly sandwich? GSA Today 12 (9), 4–10.

Jackson, J.A., Austrheim, H., McKenzie, D., Priestley, K., 2004. Metastability, mechanical strength, and the support of mountain belts. Geology 32, 625–628.

Jamieson, R.A., Beaumont, C., Medvedev, S., Nguyen, M.H., 2004. Crustal channel flows: 2. Numerical models with implications for metamorphism in the Himalayan–Tibetan orogen. J. Geophys. Res. 109, B06407. doi:10.1029/2003JB002811.

Ji, W.-Q., Wu, F.-Y., Chung, S.-L., Li, J.-X., Liu, C.-Z., 2009. Zircon U–Pb geochronology and Hf isotopic constraint on petrogenesis of the Gangdese batholith, southern Tibet. Chem. Geol. 262, 229–245.

Kapp, P., Yin, A., Harrison, T.M., Ding, L., 2005. Cretaceous–Tertiary shortening, basin development, and volcanism in central Tibet. Geol. Soc. Am. Bull. 117, 865–878.

Kay, R.W., 1978. Aleutian magnesian andesites: melts from subducted Pacific oceanic crust. J. Volcanol. Geotherm. Res. 4, 117–132.

Kay, R.W., Kay, S.M., 2002. Andean adakites: three ways to make them. Acta Petrol. Sin. 18, 303–311.

Kay, S.M., Mpodpzos, C., 2001. Central Andean ore deposits linked to evolving shallow subduction systems and thickening crust. GSA Today 11 (3), 4–9.

Kay, S.M., Mpodpzos, C., 2002. Magmatism as a probe to the Neogene shallowing of the Nazca plate beneath the modern Chilean flatslab. J. South Am. Earth Sci. 15, 39–59.

Kay, S.M., Mpodpzos, C., Ramos, V.P., Munizaga, F., 1991. Magma source variations for mid-late Tertiary magmatic rocks associated with a shallowing subduction zone and a thickening crust in the central Andes (22 to 33°S). In: Harmon, R.S., Rapela, C.W. (Eds.), Andean Magmatism and Its Tectonic Settings: GSA Spec. Paper, vol. 265, pp. 113–137.

Kay, S.M., Mpodozis, C., Tittler, A., Cornejo, P., 1994. Tertiary magmatic evolution of the Maricunga mineral belt in Chile. Int. Geol. Rev. 36, 1079–1112.

Kay, S.M., Mpodpzos, C., Coira, B., 1999. Magmatism, tectonism, and mineral deposits of the Central Andes (22°–33°S). In: Skinner, B. (Ed.), Geology and Ore Deposits of the Central Andes: Soc. Economic Geol. Spec. Publ. SEG, No. 7, pp. 27–59.

King, J., Harris, N., Argles, T., Parrish, R., Charlier, B., Sherlock, S., Zhang, H.F., 2007. First field evidence for southward ductile flow of Asian crust beneath southern Tibet. Geology 35, 727–730.

Lee, H.-Y., 2007. The Linzizong volcanic successions, southern Tibet: ages, geochemical characteristics and petrogenesis. Ph.D. thesis, National Taiwan University.

Lee, H.-Y., Chung, S.-L., Wang, J.-R., Wen, D.-J., Lo, C.-H., Yang, T.-Y.F., Xie, Y., Lee, T.-L., Wu, G., Ji, J., 2003. Miocene Jiali faulting and its implications for Tibetan tectonic evolution. Earth Planet. Sci. Lett. 205, 185–194.

Lee, H.-Y., Chung, S.-L., Wang, Y., Zhu, D., Yang, J., Song, B., Liu, D., Wu, F.-Y., 2007. Age, petrogenesis and geological significance of the Linzizong volcanic successions in the Linzhou basin, southern Tibet: evidence from zircon U–Pb dates and Hf isotopes. Acta Petrol. Sin. 23, 493–500.

Lee, H.-Y., Chung, S.-L., Lo, C.-H. Ji, J., Lee, T.-Y., Qian, Q., Zhang, Q., this volume. Eocene Neotethyan slab breakoff in southern Tibet inferred from the Linzizong volcanic record. Tectonophysics.

Liang, Y.-H., Chung, S.-L., Liu, D., Xu, Y., Wu, F.-Y., Yang, J.-H., Wang, Y., Lo, C.-H., 2008. Detrital zircon evidence from Burma for reorganization of the eastern Himalayan river system. Am. J. Sci. 308, 618–638.

Mantle, G.W., Collins, W.J., 2008. Quantifying crustal thickness variations in evolving orogens: correlation between arc basalt composition and Moho depth. Geology 36, 87–90.

Martin, H., 1999. Adakitic magmas: modern analogues of Archean granitoids. Lithos 46, 411–429.

Miller, C., Schuster, R., Klötzli, U., Frank, W., Purtscheller, F., 1999. Post-collisional potassic and ultrapotassic magmatism in SW Tibet: geochemical and Sr–Nd–Pb–O isotopic constraints for mantle source characteristics and petrogenesis. J. Petrol. 40, 1399–1424.

Murphy, M.A., Yin, A., Harrison, T.M., Dürr, S.B., Chen, Z., Ryerson, F.J., Kidd, W.S.F., Wang, X., Zhou, X., 1997. Did the Indo–Asian collision alone create the Tibetan plateau? Geology 25, 719–722.

Nomade, S., Renne, P.R., Mo, X., Zhao, D., Zhou, S., 2004. Miocene volcanism in the Lhasa Block, Tibet: spatial trends and geodynamic implications. Earth Planet. Sci. Lett. 221, 227–243.

Owens, T., Zandt, G., 1997. Implications of crustal property variations for models of Tibetan plateau evolution. Nature. 387, 37–43.

Pearce, J.A., Kempton, P.D., Nowell, G.M., Noble, S.R., 1999. Hf–Nd element and isotope perspective on the nature and provenance of mantle and subduction components in western Pacific arc–basin systems. J. Petrol. 40, 1579–1611.

Plank, T., Langmuir, C.H., 1988. An evaluation of the global variations in the major element chemistry of arc basalts. Earth Planet. Sci. Lett. 90, 349–370.

Rapp, R.P., Watson, E.B., Miller, C.F., 1991. Partial melting of amphibolite/eclogite and the origin of Archean trondhjemites and tonalities. Precambrian Res. 51, 1–25.

Royden, L.H., Burchfiel, B.C., King, W., Wang, E., Chen, Z., Shen, F., Liu, Y., 1997. Surface deformation and lower crustal flow in Eastern Tibet. Science. 276, 788–790.

Saleeby, J., Ducea, M., Clemens-Knott, D., 2003. Production and loss of high-density batholithic root, southern Sierra Nevada, California. Tectonics 22, 1064. doi:10.1029/2002TC001374.

Scherer, E., Munker, C., Merzger, K., 2001. Calibration of the lutetium–hafnium clock. Science. 293, 683–687.

Searle, M.P., Simpson, R.L., Law, R.D., Parrish, R.R., Waters, D.J., 2003. The structure geometry, metamorphic and magmatic evolution of the Everest massif, High Himalaya of Nepal–South Tibet. J. Geol. Soc. Lond. 160, 345–366.

Spicer, R.A., Harris, N.B.W., Widdowson, M., Herman, A.B., Guo, S., Valdes, P.J., Wolfe, J.A., Kelley, S.P., 2003. Constant elevation of southern Tibet over the past 15 million years. Nature. 421, 622–624.

Tapponnier, P., Xu, Z., Roger, F., Meyer, B., Arnaud, N., Wittlinger, G., Yang, J., 2001. Oblique stepwise rise and growth of the Tibet plateau. Science. 294, 1671–1677.

Thompson, A.B., Schulmann, K., Jezek, J., Tolar, V., 2001. Thermally softened continental extensional zones (arcs and rifts) as precursors to thickened orogenic belts. Tectonophysics 332, 115–141.

Turner, S., Arnaud, N., Liu, J., Rogers, N., Hawkesworth, C., Harris, N., Kelley, S., van Calsteren, P., Deng, W.-M., 1996. Post-collision, shoshonitic volcanism on the Tibetan plateau: implications for convective thinning of the lithosphere and the source of ocean island basalts. J. Petrol. 37, 45–71.

Vervoort, J.D., Patchett, P.J., Blichert-Toft, J., Albarède, F., 1999. Relationships between Lu–Hf and Sm–Nd isotopic systems in the global sedimentary system. Earth Planet. Sci. Lett. 168, 79–99.

Wen, D.-R., 2007. The Gangdese Batholith, southern Tibet: ages, geochemical characteristics and petrogenesis. Unpubl. PhD thesis, National Taiwan University.

Wen, D.-R., Chung, S.-L., Song, B., Iizuka, Y., Yang, H.-J., Ji, J., Liu, D., Gallet, S., 2008a. Late Cretaceous Gangdese intrusions of adakitic geochemical characteristics, SE Tibet: petrogenesis and tectonic implications. Lithos 105, 1–11.

Wen, D.-R., Liu, D., Chung, S.-L., Chu, M.-F., Ji, J., Zhang, Q., Song, B., Lee, T.-Y., Yeh, M.-W., Lo, C.-H., 2008b. Zircon SHRIMP U–Pb ages of the Gangdese Batholith and implications for Neotethyan subduction in southern Tibet. Chem. Geol. 252, 191–201.

Williams, H., Turner, S., Kelley, S., Harris, N., 2001. Age and composition of dikes in southern Tibet: new constraints on the timing of east–west extension and its relationship to postcollisional magmatism. Geology 29, 339–342.

Williams, H., Turner, S.P., Pearce, P.A., Kelley, S.P., Harris, N.B.W., 2004. Nature of the source regions for post-collisional, potassic magmatism in Southern and Northern Tibet from geochemical variations and inverse trace element modeling. J. Petrol. 45, 555–607.

Wright, T.J., Parsons, B., England, P.C., Fielding, E.J., 2004. InSAR observations of low slip rates on the major faults of western Tibet. Science. 305, 236–239.

Yin, A., Harrison, T.M., 2000. Geologic evolution of the Himalayan–Tibetan orogen. Annu. Rev. Earth Planet. Sci. 28, 211–280.

Zandt, G., Gilbert, H., Owens, T.J., Ducea, M., Saleeby, J., Jones, C.H., 2004. Active foundering of a continental arc root beneath the southern Sierra Nevada in California. Nature. 431, 41–46.

Zhang, H., Harris, N., Parrish, R., Kelley, S., Zhang, L., Rogers, N., Argles, T., King, J., 2004a. Causes and consequences of protracted melting of the mid-crust exposed in the North Himalayan antiform. Earth Planet. Sci. Lett. 228, 195–212.

Zhang, P.-Z., Shen, Z., Wang, M., Gan, W., Bürgmann, R., Molnar, P., Wang, Q., Niu, Z., Sun, J., Wu, J., Sun, H., You, X., 2004b. Continuous deformation of the Tibetan Plateau from global positioning system data. Geology 32, 809–812.

Zhao, W.L., Morgan, W.J., 1987. Injection of Indian crust into Tibetan lower crust: a two-dimensional finite element model study. Tectonics 6, 489–504.

Please cite this article as: Chung, S.-L., et al., The nature and timing of crustal thickening in Southern Tibet: Geochemical and zircon Hf isotopic constraints from postcollisional adakites, Tectonophysics (2009), doi:10.1016/j.tecto.2009.08.008